SYNPO2 promotes the development of BLCA by upregulating the infiltration of resting mast cells and increasing the resistance to immunotherapy

GONGJIE YE[1,2*], LINGLAN TU[3*], ZHUDUO LI[3*], XIANGYU LI[3], XIAOLIANG ZHENG[3] and YONGFEI SONG[2-4]

[1]Department of Critical Care Medicine; [2]Ningbo Institute of Innovation for Combined Medicine and Engineering, Ningbo Medical Centre Lihuili Hospital, Ningbo University, Ningbo, Zhejiang 315040; [3]School of Laboratory Medicine and Bioengineering, Hangzhou Medical College, Hangzhou, Zhejiang 310012; [4]Medical College, Ningbo University, Ningbo, Zhejiang 315211, P.R. China

Abstract. Synaptopodin 2 (SYNPO2) plays a pivotal role in regulating tumor growth, development and progression in bladder urothelial Carcinoma (BLCA). However, the precise biological functions and mechanisms of SYNPO2 in BLCA remain unclear. Based on TCGA database-derived BLCA RNA sequencing data, survival analysis and prognosis analysis indicate that elevated SYNPO2 expression was associated with poor survival outcomes. Notably, exogenous SYNPO2 expression significantly promoted tumor invasion and migration by upregulating vimentin expression in BLCA cell lines. Enrichment analysis revealed the involvement of SYNPO2 in humoral immune responses and the PI3K/AKT signaling pathway. Moreover, increased SYNPO2 levels increased the sensitivity of BLCA to PI3K/AKT pathway-targeted drugs while being resistant to conventional chemotherapy. In *in vivo* BLCA mouse models, SYNPO2 overexpression increased pulmonary metastasis of 5637 cells. High SYNPO2 expression led to increased infiltration of innate immune cells, particularly mast cells, in both nude mouse model and clinical BLCA samples. Furthermore, tumor immune dysfunction and exclusion score showed that patients with BLCA patients and high SYNPO2 expression exhibited worse clinical outcomes when treated with immune checkpoint inhibitors. Notably, in the IMvigor 210 cohort, SYNPO2 expression was significantly associated with the population of resting mast cells in BLCA tissue following PD1/PDL1 targeted therapy. In conclusion, SYNPO2 may be a promising prognostic factor in BLCA by modulating mast cell infiltration and exacerbating resistance to immune therapy and conventional chemotherapy.

Introduction

Bladder cancer is a significant global health issue, responsible for ~500,000 new cases and 200,000 deaths worldwide, with >80,000 new cases and 17,000 deaths occurring in the United States each year (1). According to clinical staging, bladder urothelial carcinoma (BLCA) is divided into two primary groups, including non-muscle-invasive urothelial carcinoma (NMIBC) and MIBC (2) . NMIBC, which constitutes ~70% of BLCA cases, is typically treated with transurethral bladder tumor resection and bladder perfusion to prevent recurrence (3). Bacillus Calmette-Guérin instillation can significantly inhibit development of NMIBC (4). A total of 20-30% of patients with MIBC undergo total cystectomy and neoadjuvant chemotherapy. Although neoadjuvant chemotherapy regimens such as Methotrexate/Vinblastine/Doxorubicin/Cisplatin (M-VAP), Capecitabine/Cisplatin and MVP have improved MIBC survival rates, their overall response rate remains at 50% (5). In advanced BLCA cases, cancer immunotherapy, such as immune checkpoint blockade, has shown promise in enhancing patient survival (6). However, due to limited molecular targets, certain patients experience unfavorable long-term outcomes. Therefore, comprehensive understanding of the molecular mechanisms and the development of novel diagnostic markers are crucial for guiding clinical BLCA management and therapy.

Synaptopodin-2 (SYNPO2), also known as Fesslin or myopodin, is localized on chromosome 4q26, contains seven exons and was first discovered in 1999 (7,8). Initially, SYNPO2 was recognized as a structural protein that serves a key role in promoting actin protein polymerization and the formation of actin bundles, facilitating creation of an F-actin network (9).

Correspondence to: Professor Xiaoliang Zheng, School of Laboratory Medicine and Bioengineering, Hangzhou Medical College, 182 Tianmushan Road, West Lake, Hangzhou, Zhejiang 310012, P.R. China
E-mail: zhengxl@hmc.edu.cn

Professor Yongfei Song, Ningbo Institute of Innovation for Combined Medicine and Engineering, Ningbo Medical Centre Lihuili Hospital, Ningbo University, 378 Dongqing Road, Yinzhou, Ningbo, Zhejiang 315040, P.R. China
E-mail: songyongfei1@gmail.com

*Contributed equally

However, studies have linked abnormal SYNPO2 expression to tumorigenesis and cancer progression: For example, De Ganck *et al* (10) showed that elevated SYNPO2 expression can stimulate the proliferation and migration of prostate cancer cells. Other investigations have suggested that SYNPO2 increases the progression of prostate cancer by regulating the formation of actin fibers and assembly of plate-like pseudopods (11,12). On the other hand, in triple-negative breast cancer, increased SYNPO2 expression is associated with enhanced tumor invasion and metastasis via its regulation of Yes-associated protein homolog 1 (YAP1) nuclear translocation (13). Yet whether SYNPO2 is a tumor suppressor or oncogene remains controversial. Roperto (14) reported that in bladder cancer infected with Bovineparvovirus (BPV), SYNPO2 upregulates molecular chaperone-mediated mitophagy, promoting cancer cell survival by binding to BAG family molecular chaperone regulator 3 (BAG3), a key autophagy protein. However, other studies have suggested that SYNPO2 may exert tumor-suppressive effects by binding to the 14-3-3 protein via importin-mediated mechanisms (9,15). These findings underscore the need for further investigation into the biological functions and molecular mechanisms of SYNPO2 in cancer, particularly in BLCA, where clarity is lacking.

The present study aims to investigate the relationship between high SYNPO2 expression and the occurrence and progression of BLCA, analyze the regulatory role of SYNPO2 in signaling pathways, and assess its impact on tumor immune infiltration.

Materials and methods

Prognostic factor selection and correlation analysis. Clinical information and RNA sequencing data of BLCA were downloaded from The Cancer Genome Atlas (cancer. gov/ccg/research/genome-sequencing/tcga, TCGA) using GDC Data Transfer Tool Version 1.6.1(docs.gdc.cancer.gov/Data_Transfer_Tool/Users_Guide/Getting_Started/#downloading-the-gdc-data-transfer-tool). Differential gene expression analysis was conducted using the DESeq2 R package Version. 1.40.2 (website: https://bioconductor.org/packages/release/bioc/html/DESeq2. html) with count data. Subsequently, next-generation sequencing data were converted into transcripts per kilobase million format for further analysis. Prognostic factors in BLCA were identified by univariate Cox regression analysis, considering factors with hazard ratio >1 and a significance level of P<0.05 as poor prognostic indicators. Independent risk factors were confirmed via multivariate Cox regression analysis. The correlation between SYNPO2 expression and clinical characteristics, such as TNM stage, subtype, histological grade and therapy, was evaluated using Kruskal-Wallis or Wilcoxon rank sum test. All statistical analyses were performed using the stats R package Version 3.4.3. (rdocumentation.org/packages/stats).

Survival analysis. All samples were categorized into low and high SYNPO2 group, based on the median SYNPO2 expression (TPM=1.703). Survival analysis was performed using Log-rank test with the survival R package Version 2.42-3 (rdocumentation.org/packages/survival). Kaplan-Meier plots were generated using the survminer R package Version 0.4.2 (rdocumentation.org/packages/survminer).

Immunohistochemistry (IHC). A total of 45 clinical BLCA samples was obtained from NingBo Medical Centre Lihuili Hospital Pathology Department (Ningbo, China). The samples were initially fixed with 4% formaldehyde, embedded in paraffin for 3 days at room temperature and cut into 4-um thick sections before deparaffinization, antigen retrieval and endogenous enzymatic activity inactivation. The sections were placed in deparaffinization solution I, II for 10 min, and III for 10 min. Subsequently, immerse the sections in absolute ethanol I for 5 min, absolute ethanol II for 5 min, and absolute ethanol III for 5 min. Finally, rinse the sections with distilled water. The sections were placed in 0.01 M citrate buffer (pH 0.6; (92℃), start the timer and maintain this temperature for 40 min. In order to inhibit endogenous peroxidase enzymes, the sections were placed in 3% hydrogen peroxide solution and incubated at room temperature in the dark for 25 min. To block non-specific binding, 10% goat serum (cat. no. C0265, Beyotime) was added for 15 min at room temperature. Tissue was incubated overnight at 4℃ with specific primary antibodies, including anti-human SYNPO2 (1:150, cat. no. 25453-1-AP), Ki67 (1:200, cat. no. 27309-1-AP), C-C chemokine receptor type 3 CCR3 (1:200, cat. no. 22351-1-AP) and Tryptase alpha/beta-1 (TPSAB1 (1:200, cat. no. 13343-1-AP; all Proteintech Group, Inc.). After washing with PBS buffer three times, sections were incubated with secondary antibody HRP-conjugated Goat Anti-Rabbit IgG (1:200, cat. no. SA00001-2, Proteintech Group, Inc.) for 2 h at 37℃. DAB staining was performed and stopped with water. Hematoxylin was used to stain the nuclei for about 3 min at 37℃, washing with tap water, hematoxylin differentiation solution for a few seconds, rinse with tap water, hematoxylin return to blue solution, and rinse. Images were obtained using a light Leica microscope at 200x magnification. Tissue staining density was assessed using Image J software Version. 1.53s (National Institutes of Health) and protein expression was analyzed by the H-score as follows: H-score=$\sum(\pi \times i)$, where i represents the intensity score (1 for weak, 2 for moderate and 3 for strong staining) and π denotes the corresponding percentage of tissue area showing each intensity.

Toluidine blue staining. Following dewaxing, place the tissue sections into Toluidine Blue staining solution (cat. no. G1032, Servicebio) at room temperature for 10-20 min. Dehydrate the sections using different concentrations of ethanol (usually 70, 95, 100%), immersing them in each concentration to ensure thorough dehydration. Clear the sections in clean xylene (cat. no.X112051, Aladdin) for 10 min, and then seal them with neutral mounting medium (cat.no. WG10004160, Servicebio). Images were collected using a light Leica microscope at 100x magnification and numbers of mast cells were calculated.

Construction of stable SYNPO2-overexpressing cell lines. Human bladder cancer cell lines T24 and 5637 were cultured in RPMI-1640 medium (cat. no. PM150110; Procell) supplemented with 10% FBS (cat. no. 164210, Procell) until the cell confluence reached 70% at 37℃ with 5% CO_2. Cell lines overexpressing SYNPO2 were generated using lentiviral vectors carrying 2.5 ug SYNPO2 cDNA or a control using Lipofectamine™ 3000 reagent (cat. no. L3000001, Invitrogen) at 37℃ for 12 h. The control plasmid was a total

of 2.5 ug pLVX-CMV-IRES-mCherry (cat. no. HH-LV-093, Hedgehogbio). Then, We performed flow cytometry to sort cells expressing mCherry three days post-transfection and identified SYNPO2 overexpression using western blotting.

Reverse transcription-quantitative (RT-qPCR). Total RNA was extracted from 5637 and T24 cell lines with SYNPO2 overexpression using RNase mini-Kit (cat. no. 74104, Qiagen GmbH) according to the manufacturer's instructions and 1 μg total RNA was reverse-transcribed using HiScript II 1st Strand cDNA Synthesis kit (cat. no. R211-01,Vazyme) according to the manufacturer's protocol. qPCR was conducted with the SYBR Green qPCR Master Mix (cat. no. QKD-201, Toyobo Life Science) using the following thermocycling conditions: Initial denaturation at 95°C for 5 min, followed by 40 cycles of 95°C for 5 sec and 55°C for 15 sec. Gene expression was normalized to the reference gene GAPDH and differences in target gene expression were calculated using the $\Delta\Delta$Cq method (16). Primer sequences were as follows: SYNPO2 forward, 5'-AGAAGCAGCCCTTACAAGTTG-3 and reverse, 5-AGCCTCACTTATTCCACTGGAT-3; GAPDH forward, 5-GGAGCGAGATCCCTCCAAAAT-3 and reverse, 5-GGCTGTTGTCATACTTCTCATGG-3; MYC forward, 5-GGCTCCTGGCAAAAGGTCA-3 and reverse, 5'-CTGCGTAGTTGTGCTGATGT-3; CDK4 forward, 5-ATGGCTACCTCTCGATATGAGC-3 and reverse, 5-CATTGGGGACTCTCACACTCT-3; CDK6 forward, 5-GCTGACCAGCAGTACGAATG-3 and reverse, 5-GCACACATCAAACAACCTGACC-3'; TP53 forward, 5'-CAGCACATGACGGAGGTTGT-3' and reverse primer, 5-TCATCCAAATACTCCACACGC-3; KRAS forward, 5-ACAGAGAGTGGAGGATGCTTT-3 and reverse, 5-TTTCACACAGCCAGGAGTCTT-3; P27 forward, 5-AACGTGCGAGTGTCTAACGG-3 and reverse, 5-CCCTCTAGGGGTTTGTGATTCT-3 and Cyclin D1 CCND1 forward, 5-TCTACACCGACAACTCCATCCG-3 and reverse, 5-TCTGGCATTTTGGAGAGGAAGTG-3'.

Western blotting. Following digestion with 0.25% trypsin (cat. no. T1320, Solarbio), the cells were collected by centrifugation at 500 g for 10 min. Protein lysate was extracted using RIPA buffer (cat. no. R0010, Solarbio) supplemented with protease inhibitor cocktail (cat. no. HY-K0010, MCE). Total protein concentration was determined using the BCA method (cat. no. P0012, Beyotime). After separation by SDS-PAGE on a 10% gel, a total of 20 ug proteins in each lane were transferred onto PVDF membranes using a transfer buffer containing 20% methanol. PVDF membranes were blocked with 10% skimmed milk at 4°C for 1 h and incubated with primary antibodies in 5% non-fat milk at 4°C overnight. The primary antibodies were as follows: Anti-human GAPDH (1:3,000, cat. no. 60004-1-Ig, Proteintech Group, Inc.), E-cadherin(1:1,000, cat. no. 610405, BD Transduction Laboratories™; BD Biosciences) and vimentin (1:1,000, cat. no. AF7013, Affinity Biosciences). Following primary antibody incubation at 4°C overnight, membranes were treated with HRP-conjugated anti-mouse (cat. no. SA00001-1) or anti-Rabbit IgG (both 1:5,000, cat. no. SA00001-2, both Proteintech Group, Inc.) for 2 h at room temperature. ECL kit (cat. no. RPN2235, Amersham) was used to visualize the protein bands. Blotted bands were detected using the GE Detecting System and analyzed using Image J software Version. 1.53s.

Wound healing assay. 5637 and T24 cells were seeded in 6-well plates with 3% FBS at 37°C. A wound scratch experiment was continued when the cell confluence reached ~90%. Wound scratch assay was conducted at 37°C using the light Leica Live Cell Imaging System (Essen Bioscience) at 10x magnification at 0 and 24 h after the scratch.

Transwell assay. A total of 10^5 cells were seeded into the upper chamber of RPMI-1640 medium without serum. Prior to seeding, T24 cells (cat. no. CL-0227, Procell) and 5637 cells (cat. no. CL-0002, Procell) were serum-starved for 4 h at 37°C in RPMI-1640 medium (cat. no. PM150110, Procell). These cells were then plated into 8 μm inserts coated with Matrigel Matrix (1:200, cat. no. 356234, Corning, Inc.) and cultured in RPMI-1640 medium (cat. no. PM150110, Procell) without fetal bovine serum. The Matrigel Matrix coating process involved melting Matrigel Matrix at 4°C overnight. RPMI-1640 medium (cat. no. PM150110, Procell) containing 10% fetal bovine serum (cat. no. 164210, Procell) was added to the lower chamber. The induction process continued for 24 h at 37°C with 5% CO_2, allowing the cells to migrate from the upper chamber through the membrane to the outside. The upper chamber was stained with crystal violet at room temperature for 1 h, following the manufacturer's instructions (cat. no. C0121, Beyotime Institute of Biotechnology). Images were captured using a Leica light microscope at 100x magnification.

Animal model. The cell lines 5637 and T24 are prominent models in the study of bladder cancer. 5637 is notable for its robust tumorigenicity, rendering it suitable for *in vivo* animal experimentation. A stable 5637 cell line expressing Luciferase was established by transfection with 2.5 ug of pLenti-CMV-Puro-LUC (pLV-Luc) plasmid (cat. no. 17477, Addgene) using Lipofectamine™ 3000 reagent (cat. no. L3000001, Invitrogen) at 37°C for 12 h, and selected by 1ug/ml puromycin (cat. no. P8230, Solarbio) for two weeks. The lentivirus packaging plasmids were used in the following ratio for each 10 mm^2 dish: pLVX-CMV-SYNPO2-IRES-mCherry (cat. no. HH-LV-093, Hedgehogbio):psPAX2 (cat. no. HH-LV-012, Hedgehogbio):pMD2.G (cat. no. HH-LV-013, Hedgehogbio)=5(10 ug):3(6 ug):1(2 ug). These plasmids were transfected into the 293-cell line at 37°C for 12 h (cat. no. CL-0001, Procell) using Lipofectamine™ 3000 reagent (catalog no. L3000001, Invitrogen). Three days following transfection, lentiviral particles were harvested by centrifugation at 50,000 g for 2 h at 4°C. The collected lentiviral particles were then resuspended in 100 ul of PBS and stored at -80°C. Then, 10 ul of 2nd lentivirus carrying SYNPO2 was employed to infect 5637 cell line expressing Luciferase. This led to the generation of another stable cell line co-expressing SYNPO2 and Luciferase, achieved through flow cytometry sorting. For *in vivo* experiments, 6x10⁶ 5637 cells co-expressing pLV-Luc and pLVX-CMV-SYNPO2-IRES-mcherry were injected into the tail veins of 6-week-old BALB/c nude mice (Charles river), with a total of 11 female mice weighing 18-22 g. The laboratory mice are housed under controlled conditions, including a temperature range of 20-24°C, humidity levels between 40 and 60%, a 12-h light/dark cycle, and continuous access to food and water to ensure their well-being during research. Tumor growth was monitored every 6 weeks by bioluminescence

imaging using an IVIS Spectrum device (PerkinElmer, Inc.) after intraperitoneal injection of 30 mg D-luciferin. Tumors did not exceed a volume of 2,000 mm^3 and diameter of 20 mm.

Immunofluorescence. Mice were euthanized by CO_2 displacement at a controlled rate of 30% container volume/min. This method ensures a gradual and controlled administration of CO_2, leading to a rapid loss of consciousness and minimal distress to minimize animal suffering. Fresh lung tissue was promptly collected and fixed in 4% paraformaldehyde at 4℃ overnight. After fixation, the tissue was washed three times with PBS buffer and soaked overnight at 4℃ in a solution containing 20% sucrose and 0.05% NaN_3. The samples were directly affixed to sample stages coated with optimal cutting temperature compound and frozen in an ice cutter at -80℃. Subsequently, frozen tissue was sectioned into 4-μm sections and mounted onto slides. Tissue sections were incubated with the primary antibody [mast cell chymase (CMA) 1; 1:200, cat. no. DF12290, Affinity Biosciences] at 4℃ overnight. They were then incubated with the secondary FITC-conjugated anti-Rabbit IgG (1:400, cat. no. SA00003-2, Proteintech Group, Inc.) at 37℃ for 1 h. DAPI staining was used to visualize the distribution of cell nuclei for 15 min at 37℃. Images were acquired using a Leica SP8 confocal microscope (magnification of 200x, and ImageJ Version. 1.53s (National Institutes of Health) was utilized to quantify the number of infiltrating mast cells.

ELISA. 800 ul Blood was extracted from BALB/c nude mice. Serum was obtained through centrifugation at 500 x g, 4℃, for 10 min. Serum concentrations of mast cell-secreted cytokines were determined using TGF-β and IL-6 ELISA kits according to their manufacturer's instructions (cat. nos. 70-EK981-48 and 70-EK206HS-48, respectively; both Hangzhou Lianke Biotechnology Co., Ltd.).

Gene Ontology (GO), Kyoto Encyclopedia of Genes and Genomes (KEGG) and Gene Set Enrichment Analysis (GSEA). A gene expression ranking matrix was generated using the DEseq2 package (17). GO, KEGG and GSEA enrichment analysis were performed using the R package ClusterProfiler Version. 4.4.4 (18). The top 10 signaling pathways from each enrichment analysis were visualized using the R package ggplot2 Version 3.4.3 (cran.r-project.org/web/packages/ggplot2/index.html). P.adj <0.05 and false discovery rate <0.25 were considered to indicate significant enrichment.

Evaluation of the sensitivity of chemotherapeutic agents. Drug sensitivity of patients was predicted using half-maximal inhibitory concentration (IC_{50}) and RNA-sequence data was obtained from TCGA. IC_{50} was calculated using the R package pRRophetic with ridge regression (19).

Assessment of correlation between SYNPO2 expression and immune infiltration. The significance and percentage of immune cells infiltrating the tumor were estimated by the xCell method based on a single-sample GSEA (ssGSEA) model (20). Expression of immune checkpoint genes in both high and low SYNPO2 groups was evaluated and correlation between the expression of each gene and SYNPO2 was assessed using

Pearson correlation analysis Tumor Immune Dysfunction and Exclusion (TIDE) model (21) was used to assess the effects of immune therapy in each group.

Evaluation of the effect of SYNPO2 expression on the response to PDL-1-targeted immune therapy. A total of 348 samples, including RNA-seq data and clinical information, was acquired from the IMvigor 210 dataset (22). CIBERSORT analysis was used to assess the association between SYNPO2 expression and human immune cell populations using IOBR R package Version 3 (github.com/IOBR/IOBR). In addition, the distribution of SYNPO2 expression in three immune infiltrating subtypes, including desert, excluded and inflamed, was detected.

Statistical analysis. Statistical analysis was performed using R version 3.6.1 software (Website: https://cran.utstat.utoronto.ca/bin/windows/base/old/3.6.1/). The data are presented as mean ± standard error of the mean (SEM). Paired Student and Welch t and Wilcoxon's rank-sum test were applied to compare two groups, while the Kruskal-Wallis test with multiple hypothesis testing (Dunn's post hoc test) was performed to compare multiple groups. Each experiment was repeated three times. P<0.05 was considered to indicate a statistically significant difference.

Results

High SYNPO2 expression is a poor prognostic factor in BLCA. Univariate and multivariate Cox proportional hazards analysis (Table I) revealed high SYNPO2 expression as an independent risk factor associated with poor prognosis in patients with BLCA. Survival analysis further supported these findings, indicating an association between elevated SYNPO2 levels and shorter overall and progression-free survival and increased mortality (Fig. 1A-C). SYNPO2 expression was correlated with BLCA progression, including clinical pathological, T and N stage (Fig. 1D-F). Notably, SYNPO2 expression was significantly lower in papillary compared with non-papillary bladder cancer (Fig. 1G), while higher SYNPO2 levels were detected in bladder cancer cases with lympho-vascular invasion than those without (Fig. 1H). In addition, in 45 clinical cancer samples from patients with BLCA, IHC revealed a positive correlation between SYNPO2 expression and oncogene Ki67 (Fig. 1I and J). In a prognosis model for BLCA, SYNPO2 expression was inversely associated with the 1- and 3-year survival rates. Higher total scores in this model signified an increased mortality risk (Fig. 1K). Overall, these results underscore the role of SYNPO2 as a risk factor associated with BLCA development.

SYNPO2 overexpression promotes the invasion and migration of BLCA cell lines. RT-qPCR was used to detect mRNA levels of proliferation-associated genes, including MYC (23), KRAS (24), TP53 (25), P27 (26), CDK4, CDK6 (27) CCND1 (28) and SYNPO2. SYNPO2 overexpression increased the levels of oncogene C-MYC in both 5637 (n=3) and T24 (n=3) cell lines (Fig. 2A and B). Transwell invasion assay demonstrated that SYNPO2 overexpression significantly increased the invasive capacity of BLCA 5637 (n=3) and T24

Table I. Univariate and multivariate Cox proportional hazards analysis between SYNPO2 expression and overall survival for patients with Bladder Urothelial Carcinoma (BLCA).

Characteristic	n	Univariate analysis		Multivariate analysis	
		Hazard ratio (95% CI)	P-value	Hazard ratio (95% CI)	P-value
T stage [T1&2 (n=124) vs. T3&4 (n=255)]	379	2.199 (1.515-3.193)	<0.001[a]	0.914 (0.203-4.123)	0.907
N stage [N0&1 (n=285) vs. N2&3 (n=84)]	369	2.273 (1.640-3.150)	<0.001[a]	2.050 (0.908-4.632)	0.084
M stage [M0 (n=202) vs. M1 (n=11)]	213	3.136 (1.503-6.544)	0.002[a]	0.696 (0.180-2.695)	0.600
Pathological stage [I&II (n=134) vs. III&IV (n=277)]	411	2.310 (1.596-3.342)	<0.001[a]	1.872 (0.334-10.492)	0.476
Radiation therapy [no (n=366) vs. yes (n=21)]	387	0.965 (0.475-1.964)	0.923		
Sex [female (n=109) vs. male (n=304)]	413	0.849 (0.616-1.169)	0.316		
Ethnicity [Asian&Black or African American (n=67) vs. White (n=329)]	396	1.145 (0.731-1.794)	0.554		
Weight [≤80 (n=204) vs. >80 kg (n=166)]	370	0.968 (0.709-1.323)	0.840		
Height [≤170 cm (n=158) vs. >170 cm (n=206)]	364	1.100 (0.798-1.518)	0.561		
BMI [≤25 (n=152) vs. >25 (n=211)]	363	0.978 (0.706-1.353)	0.892		
Histological grade [high (n=389) vs. low (n=21)]	410	0.337 (0.083-1.360)	0.126		
Smoking status [no (n=109) vs. yes (n=291)]	400	1.305 (0.922-1.847)	0.133		
Primary therapy outcome	357	0.226 (0.162-0.315)	<0.001[a]	0.455 (0.218-0.949)	0.036[a]
[PD&SD (n=101) vs. PR&CR (n=256)]	413	1.421 (1.063-1.901)	0.018[a]	1.428 (0.727-2.803)	0.301
Age [≤70 (n=233) vs. >70 years (n=180)]	408	0.690 (0.488-0.976)	0.036[a]	1.635 (0.737-3.628)	0.226
Subtype [non-papillary (n=275) vs. papillary (n=133)]					
Lymphovascular invasion	282	2.294 (1.580-3.328)	<0.001[a]	1.677 (0.732-3.843)	0.222
[no (n=130) vs. yes (n=152)]	413	1.609 (1.195-2.168)	0.002[a]	2.238 (1.093-4.582)	0.028[a]
SYNPO2 expression [low (n=207) vs. high (n=206)]					

[a]P<0.05. BMI, body mass index; PD, progressive disease; SD, Stable disease; PR, Partial response; CR, Complete response; SYNPO2, Synaptopodin-2. Bold text represents P<0.05.

cell lines (n=3; Fig. 2C and D). Additionally, scratch assay revealed that SYNPO2 overexpression increased wound healing in BLCA cell lines (n=3, Fig. 2E and F).

In cancer cells with high metastatic potential, expression of vimentin protein is typically upregulated, while E-cadherin protein is inhibited (29). Western blotting showed increased vimentin levels in the 5637 cell line with SYNPO2 overexpression (Fig. 2G and H). To validate the metastasis and invasion-promoting effects of SYNPO2, a BLCA lung metastasis model was established in nude mice (n=11) via. intravenous tail injection (Fig. 2I). While the association between SYNPO2 overexpression and survival of this model was not significant, SYNPO2 increased the risk of death (HR=2.354, 95% CI:0.4726-11.73; Fig. 2J). *In vivo* imaging analysis revealed that the area of BLCA metastasis in the SYNPO2 overexpression group was ~2-fold larger than that in the control group at 6 weeks and ~4-fold larger at 12 weeks (Fig. 2K).

SYNPO2 regulates innate immune-associated and PI3K/AKT signaling pathways. To uncover the molecular mechanisms of by SYNPO2 in cancer development, BLCA next-generation sequencing data was obtained from TCGA database. Utilizing DESeq2 analysis, differentially expressed genes (DEGs; |logFC|>2, P<0.05) between SYNPO2 expression groups were obtained, comprising 2,422 upregulated and 513 down-regulated genes. The top 10 genes are shown (Fig. 3A). GO) analysis revealed that abnormal SYNPO2 expression led to dysfunction in the innate immune system across biological processes including 'complement activation', 'formation of immunoglobulin complexes' and 'antigen-binding process', cell components and molecular functions (Fig. 3B-D). KEGG pathway analysis highlighted the top 10 enriched pathways, including 'neuroactive ligand-receptor interaction', 'PI3K-Akt signaling pathway', 'cytokine-cytokine receptor interaction', 'MAPK signaling pathway', 'calcium signaling pathway', 'cAMP signaling pathway', 'regulation of actin cytoskeleton', 'focal adhesion', 'protein digestion and absorption' and 'vascular smooth muscle contraction' (Fig. 3E). GSEA also showed the enrichment of the 'PI3K-AKT signaling pathway' (Fig. 3F). Overall, these findings suggested that SYNPO2 expression modulated innate immune-related and the PI3K/AKT signaling pathway.

SYNPO2 expression increases the sensitivity of PI3K/AKT-targeted drugs. Given that survival in patients with BLCA at the advanced stage depends on drug response (30), drug sensitivity of BLCA in different SYNPO2 expression groups was evaluated based on RNA-sequencing data from TCGA database. IC_{50} prediction indicated that SYNPO2
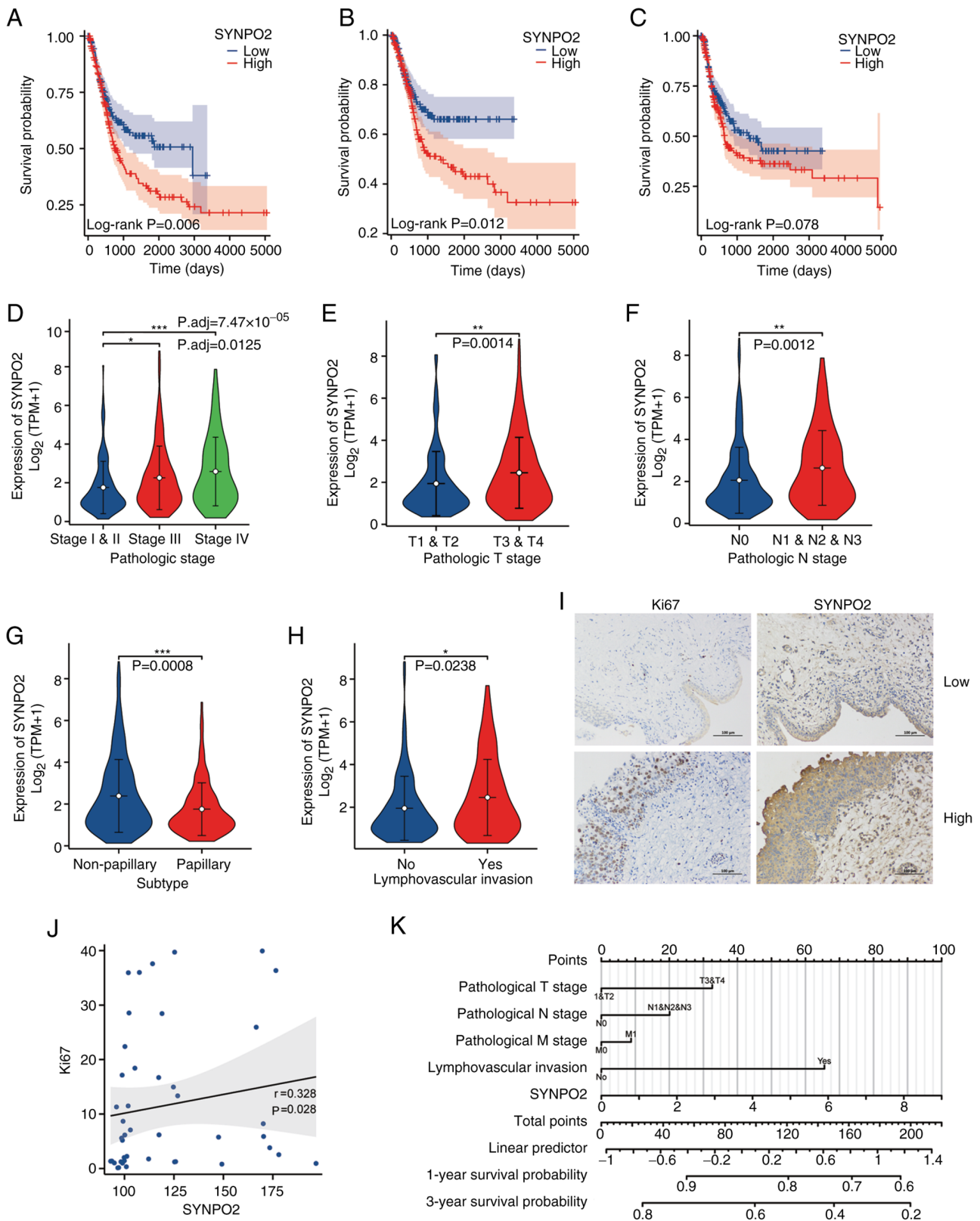
Figure 1. High SYNPO2 expression is a poor prognostic factor in BLCA. (A) Overall survival in patients with BLCA with low (n=206) and high (n=205) SYNPO2 expression. (B) Disease-specific survival in patients with BLCA in low (n=200) and high (n=179) SYNPO2 expression groups. (C) Progression-free interval for patients based on SYNPO2 expression (low, n=206; high, n=206). (D) Distribution of SYNPO2 expression in BLCA samples from patients at different stages. Stage I and stage II (n=133), stage III (n=142), stage IV (n=135). Stage I and II vs. stage III, P.adj=0.0125, stage I and II vs, stage IV P.adj=7.47x1005. (E) Distribution of SYNPO2 expression in patients with BLCA at different T stages. T1 and T2 (n=123) vs. T3 and T4 (n=255), P=0.0014. (F) SYNPO2 expression in patients with BLCA at different N stages. N0 (n=238) vs. N1, N2 and N3 (n=130), P=0.0012. (G) SYNPO2 expression in BLCA samples of non-papillary (n=273) and papillary (n=134) subtypes. P=0.0008. (H) SYNPO2 expression in patients with BLCA with (n=129) or without (n=152) lymphovascular invasion. P=0.0238. (I) Representative immunohistochemistry of Ki67 and SYNPO2 staining in BLCA tissue with low and high SYNPO2 expression. (J) Spearman correlation analysis of Ki67 and SYNPO2 expression (n=45). (K) Nomogram based on multivariate Cox regression analysis for 1 and 3-year survival probability. SYNPO2, synaptopodin-2; BLCA, Bladder Urothelial Carcinoma; TPM, Transcript per million. *, ** and *** indicate P<0.05, P<0. 01, P<0.001, respectively.
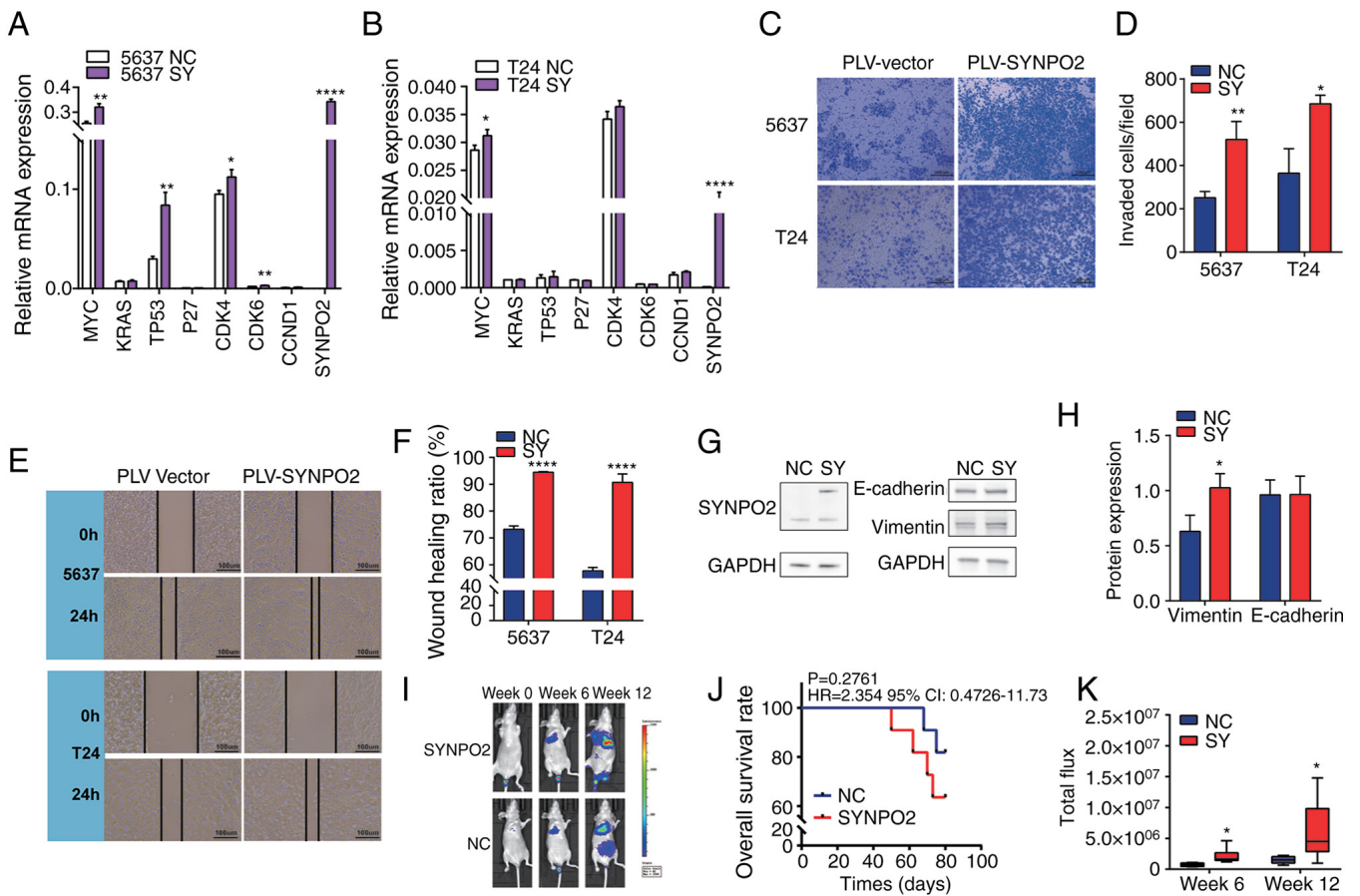
Figure 2. SYNPO2 overexpression increases invasion of BLCA *in vivo* and *in vitro*. (A) mRNA levels in NC and SYNPO2-overexpressing 5637 cells was detected by reverse transcription-quantitative PCR. MYC, P=0.0019; TP53, P=0.0023; CDK4, P=0.0221; CDK6, P=0.0022 and SYNPO2, P<0.0001 between NC and SY group. (B) mRNA levels in T24 cells. MYC, P=0.0343 and SYNPO2, P<0.0001 between NC and SY group. (C) Transwell invasion assay of BLCA cell lines with SYNPO2 overexpression. (D) Number of invaded 5637 (P=0.006) and T24 cells (P=0.0101). (E) Representative (F) wound healing assay in 5637 or T24 cells at 0 and 24 h. (G) Western blotting analysis for (H) SYNPO2, E-cadherin, vimentin and GAPDH protein. Vimentin, P=0.025. (I) Bioluminescence imaging of 5637-Luc cells at 0, 6 and 12 weeks. (J) Kaplan-Meier survival analysis of nude mice implanted with 5637-Luc cells. (K) Total flux in each group *in vivo* imaging. 6 week NC (n=6) vs. SY (n=6), P=0.0247; 12 week NC (n=6) vs. SY (n=5), P=0.0445. SYNPO2, Synaptopodin-2; BLCA, Bladder Urothelial Carcinoma; NC, Negative Control; SY, SYNPO2 overexpression; Luc, Luciferase. *, ** and **** indicate P<0.05, P<0.01, P<0.0001, respectively.

expression increased resistance to conventional chemotherapeutic drugs, including docetaxel, paclitaxel, doxorubicin and gemcitabine (Fig. 4A-D).

The PI3K/AKT signaling pathway plays a vital role in tumorigenesis and is one of the important therapeutic targets in the treatment of several types of cancer (31). Various molecules in this pathway, such as c-met, AKT1/2/3, PI3K, mTOR and VEGFR, are involved, and drugs targeting them, including crizotinib, MK-2206, AZD8055, rapamycin and sorafenib, have been employed in clinical therapy (32-35). Therefore, sensitivity of these PI3K-AKT targeted drugs was assessed. IC_{50} of these drugs in BLCA with high SYNPO2 expression was significantly decreased compared with the low SYNPO2 group (Fig. 4E-I).

SYNPO2 expression facilitates mast cell infiltration in BLCA. Given the potential impact of SYNPO2 expression on immune function (36,37), ssGSEA was used to estimate tumor immune infiltration levels. Several innate immune cell types, including mast (r=0.636) and natural killer (NK) cells (r=0.509) and eosinophils (r=0.489), exhibited significant correlations with SYNPO2 expression (Fig. 5A). To validate the role of SYNPO2

in increasing mast cell infiltration in BLCA tissues, mast cell degranulation and protein expression in BLCA tissue was measured using IHC and toluidine blue staining. Toluidine blue staining revealed a significantly higher number of mast cells in BLCA tissues with high SYNPO2 expression (Fig. 5B and C). Additionally, TPSAB1 staining, a mast cell marker, showed a positive association between SYNPO2 expression and TPSAB1 levels (r=0.708; Fig. 5B and D). Moreover, the levels of the mast cell surface receptor CCR3 (r=0.623) also strongly correlated with SYNPO2 expression (Fig. 5B and E).

In the *in vivo* model, SYNPO2 overexpression increased lung metastasis of BLCA, as evidenced by a significant increase in mast cells expressing CMA1 in the immunofluorescence assay (Fig. 5G and I). Furthermore, mast cell-secreted immune suppressive cytokines, including TGF-β1 and IL-6, were significantly higher in the SYNPO2 overexpression group compared with the control (Fig. 5F and H).

SYNPO2 increases immunotherapy resistance by upregulating infiltration of resting mast cells. To assess the association between SYNPO2 and immunotherapy, expression levels of eight immune checkpoint-associated genes (38), including
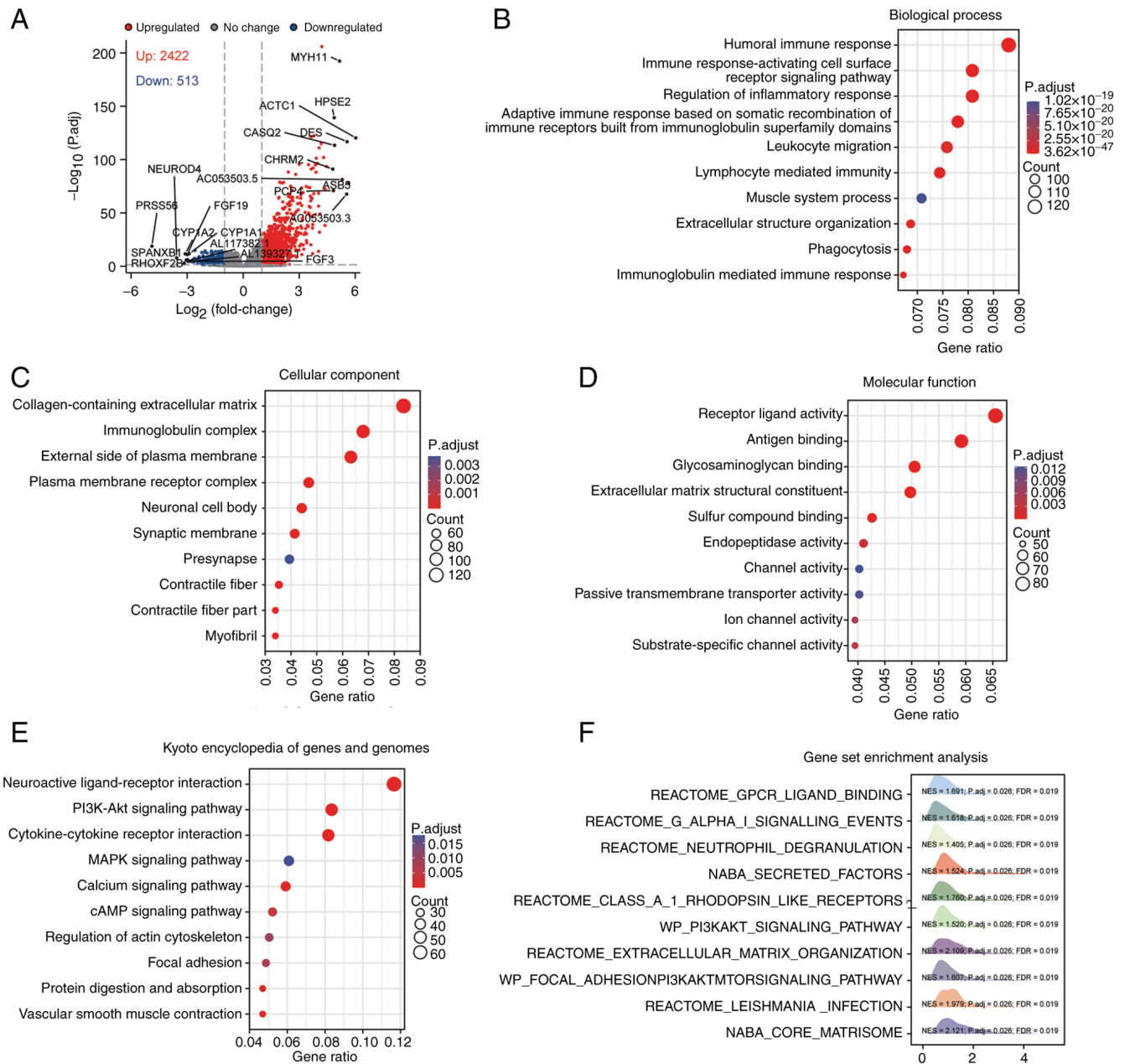
Figure 3. Abnormal SYNPO2 expression regulates multiple signaling pathways. (A) DEGs in BLCA samples with high and low SYNPO2 expression (n=206). Top 10 enriched Gene Ontology terms for (B) biological process, (C) cellular component and (D) molecular function. (E) Top 10 signaling pathways enriched by Kyoto Encyclopedia of Genes and Genomes. (F) Top 10 Gene Set Enrichment Analysis pathways. SYNPO2, synaptopodin-2; DEG, Differential Expression Genes; BLCA, Bladder Urothelial Carcinoma.

programmed cell death protein 1 (PDCD1), Lymphocyte activation gene 3 protein, CD274, hepatitis A virus cellular receptor 2 (HAVCR2), cytotoxic T-lymphocyte protein 4 (CTLA4), programmed cell death 1 ligand 2 (PDCD1LD2), T-cell immunoreceptor with Ig and ITIM domains (TIGIT) and sialic acid-binding Ig-like lectin 15 (SIGLEC15), were evaluated using RNA-seq data from TCGA database. Except for CD274 and SIGLEC15, expression of immune checkpoint genes was correlated with SYNPO2 levels (Fig. 6A). Additionally, to predict the response to ICIs, TIDE score was calculated. In the high SYNPO2 expression group, TIDE score was significantly higher compared with the low SYNPO2 expression group, indicating that SYNPO2 expression increased resistance to ICIs (Fig. 6B).

ICIs are developed based on the concept of reactivating preexisting anti-tumor T cell responses suppressed due to inherent immunological resistance in BLCA (39). To validate the current hypothesis that SYNPO2 expression affects the efficacy of immune therapy in BLCA we evaluated immune microenvironment subtypes and infiltration in a cohort of 348 BLCA patients who were treated with atezolizumab, a PD-L1 inhibitor. This analysis was based on the data from the IMvigor 210 study, which included RNA-sequencing data and clinical information. Among the three subtypes of immune infiltration, the excluded subtype exhibited higher SYNPO2 expression compared with the desert subtype (P=0.0023; Fig. 6C). According to analysis of immune cell infiltration, SYNPO2 expression was positively correlated with infiltration
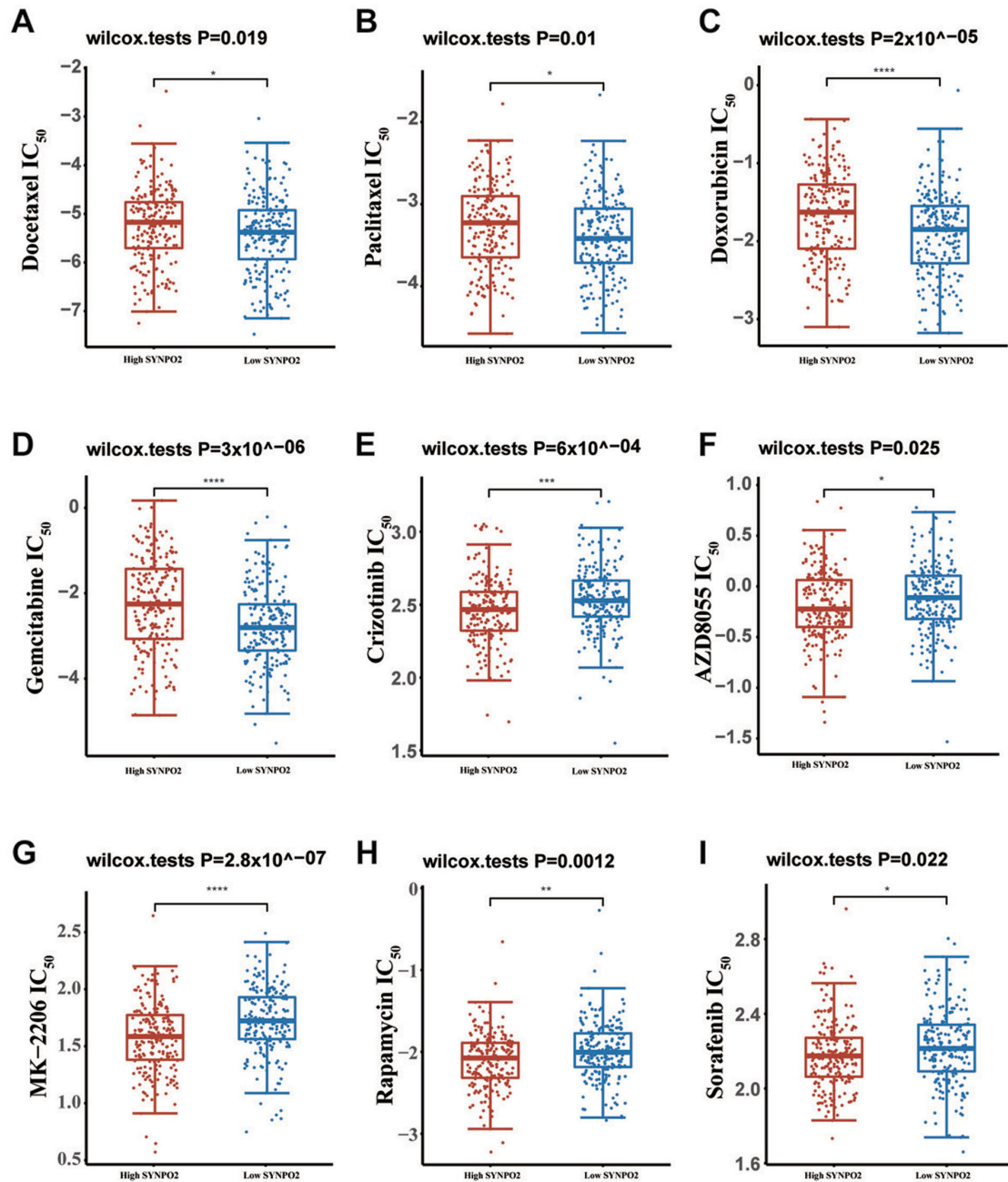
Figure 4. Drug sensitivity in bladder Urothelial Carcinoma (BLCA) with different SYNPO2 expression. IC_{50} of (A) docetaxel, P=0.019 (B) paclitaxel, P=0.01 (C) doxorubicin, $P=2x10^{-05}$ (D) gemcitabine, $P=3x10^{-06}$ (E) crizotinib, $P=6x10^{-04}$ (F) AZD8055, P=0.025 (G) MK-2206, $P=2.8x10^{-07}$ (H) rapamycin P=0.0012 and (I) sorafenib P=0.022. IC_{50}, half maximal inhibitory concentration; SYNPO2, Synaptopodin-2. *, **, *** and **** indicate P<0.05, P<0.01, P<0.001, P<0.0001, respectively.

of mast cells at rest (R=0.146), monocytes (R=0.209) and resting CD4 memory T cells (r=0.284), while it was negatively correlated with activated mast cell infiltration (R=-0.212; Fig. 6D-G). Therefore, SYNPO2 may increase resistance to immunotherapy by upregulating the infiltration of resting mast cells.

Discussion

In numerous cancer types, SYNPO2 exhibits different effects. For example, in triple-negative breast cancer (TNBC) and colorectal cancer, SYNPO2 is reported to act as a tumor suppressor by reducing TNBC metastasis and inhibiting proliferation and migration in colorectal cancer by regulating specific molecular pathways (40,41). However, in prostate cancer, SYNPO2 overexpression is associated with enhanced cell migration, potentially due to its involvement in stress fiber assembly (10,15). The present findings align with previous studies, suggesting that SYNPO2 is an independent predictor of poor clinical outcome and is positively linked to increased metastasis in cancer (37,42). Notably, drug resistance poses a challenge in the treatment of patients with advanced BLCA. A study reported that TEA domain family member 4 promotes BLCA invasion by activating epithelial-mesenchymal transition via the PI3K/AKT pathway (43,44). Here, high SYNPO2 expression correlated with resistance to conventional
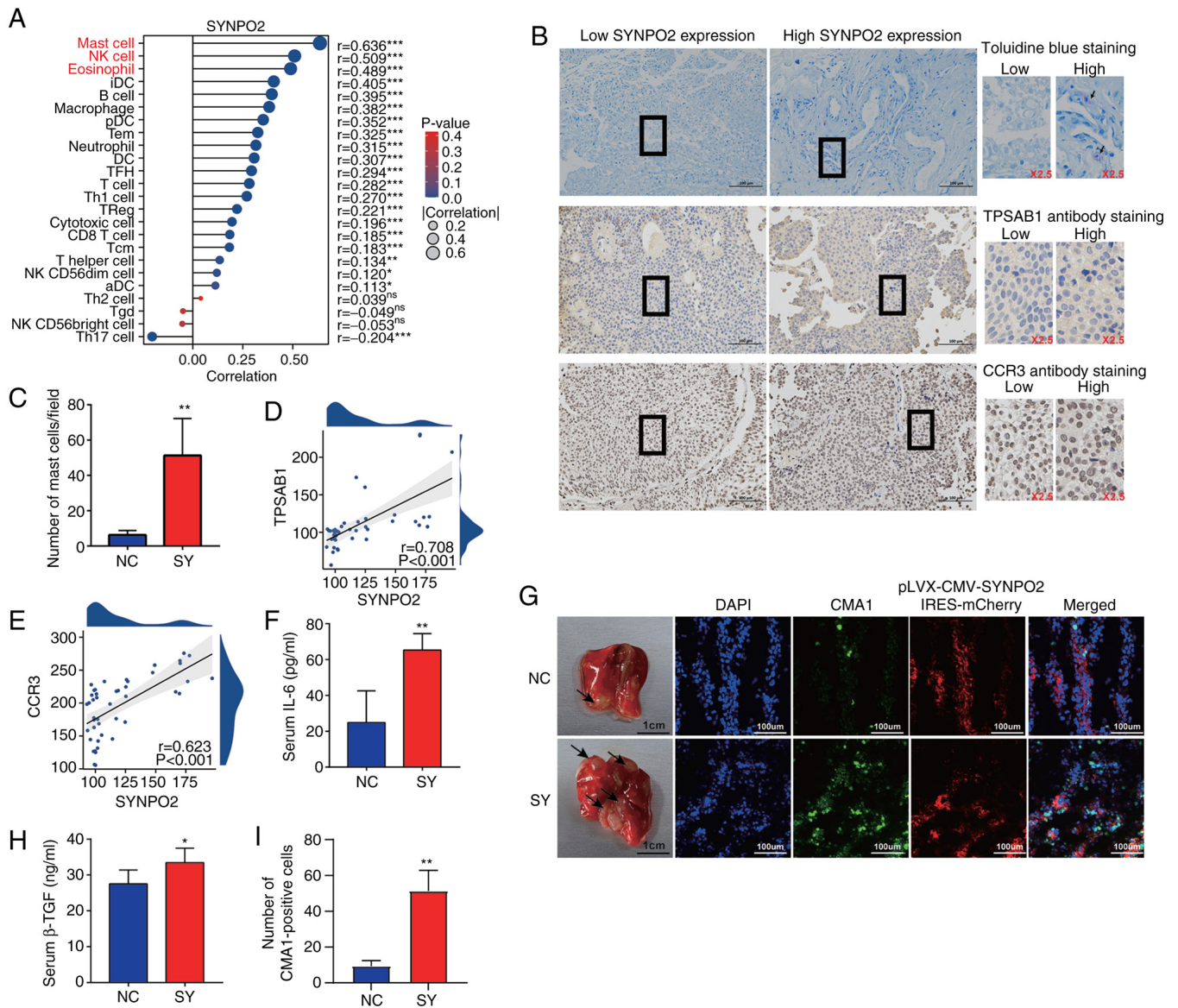
Figure 5. SYNPO2 expression enhances mast cell infiltration. (A) SYNPO2 expression in 24 types of immune cell. Red text indicates a high correlation. (B) Representative toluidine and immunohistochemical staining in clinical Bladder Urothelial Carcinoma (BLCA) samples with low and high SYNPO2 expression. Purple represents cell degranulation. Scale bar, 100 μm. (C) Mast cell number/field in low and high SYNPO2 expression groups (P=0.0053). Correlation between SYNPO2 and (D) TPSAB1 and (E) CCR3 expression based on H-score. (F) Mouse serum IL-6 levels in NC (n=5) and SY (n=5; P=0.002). (G) Representative indirect immunofluorescence of a frozen lung section from a mouse model with pulmonary metastasis. The black arrow indicates the area of tumor invasion in the lung tissue. (H) Mouse serum TGF-β1 levels (P=0.045). (I) CMA-positive cells (n=3, P=0.0036). SYNPO2, synaptopodin-2; TPSAB1, Tryptase alpha/beta-1; CCR3, C-C chemokine receptor type 3; NC, Negative Control; SY, SYNPO2 overexpression; CMA1, Chymase 1. * and ** indicate P<0.05, P<0.01, respectively.

chemotherapy agents such as paclitaxel, cisplatin and doxorubicin and increased sensitivity to PI3K/AKT-targeted drugs, suggesting that patients with high SYNPO2 expression may benefit more from targeted therapies such as rapamycin, MK-2206 and AZD8055 (Fig. 7).

Immune cell infiltration serves a crucial role in tumor progression by shaping the BLCA microenvironment. Innate immune cells participate in immune suppression, inhibiting adaptive immune responses in the early stages of tumor development (45). For example, mast cells stimulate IL-17 secretion from myeloid-derived suppressor cells, leading to IL-9 release from regulatory T (Treg) cells, thereby promoting tumor growth in the microenvironment (46). The present study observed significant correlations between SYNPO2 expression and infiltration of various innate immune cells, including mast cells, eosinophils, NK cells, immature dendritic Cells (iDC), B cells, macrophages, plasmacytoid dendritic cell (pDC), follicular helper T cell (TFH), DC, neutrophils and memory T cell (Tem) and T cells. GO analysis revealed that SYNPO2 was involved in multiple classical pathways associated with innate immune regulation, such as complement activation, formation of immunoglobulin complexes and antigen-binding process. Therefore, SYNPO2 can induce the infiltration of suppressive innate immune cells, thereby increasing BLCA development and progression via the regulation of immune-associated signaling pathways.

Mast cells are innate immune cells commonly found in connective tissue near lymphatic systems, blood vessels, skin
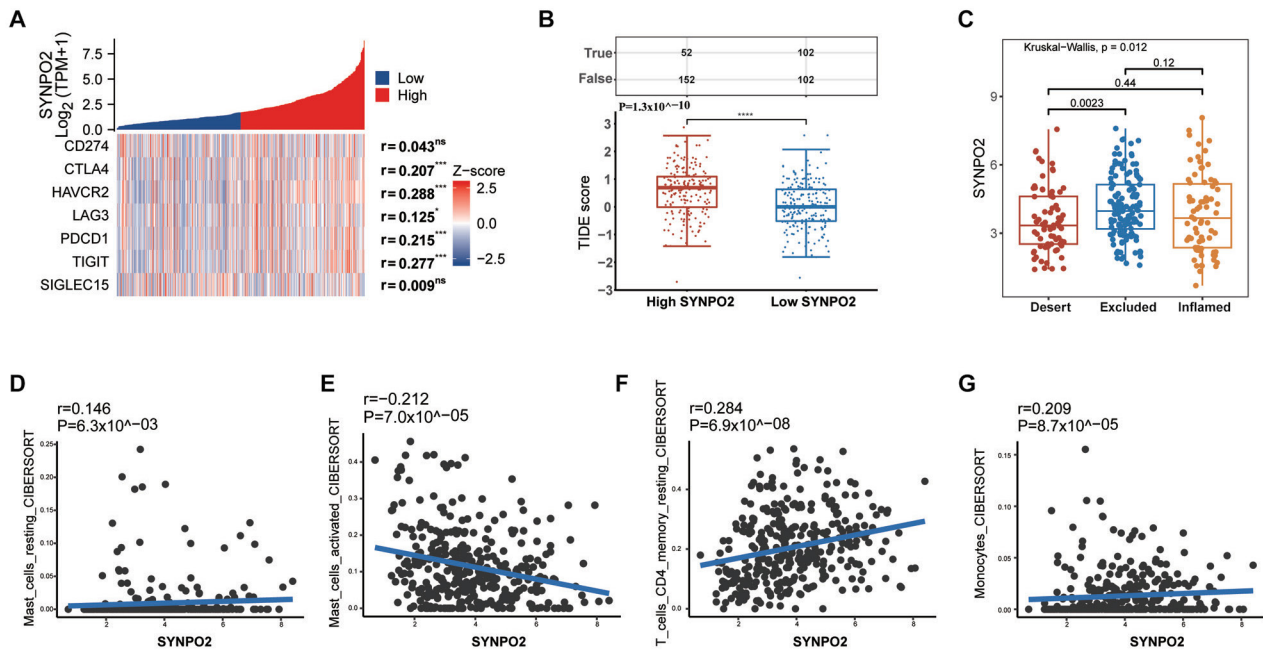
Figure 6. High SYNPO2 expression increases resistance to anti-PDL1 immune therapy. (A) Correlation of immune checkpoint genes with SYNPO2. (B) TIDE score. True presents numbers of positive immune responses; False presents numbers of negative immune responses; Red, resistance to immune checkpoint blocking; blue, positive response, $P=P=1.3 \times 10^{-10}$. (C) Differences in SYNPO2 expression in three immune infiltration types, The Deserted *VS* The Excluded $P=0.0023$. Correlation between SYNPO2 and (D) resting, $P=6.3 \times 10^{-03}$ and (E) activated mast cell, $P=7.0 \times 10^{-05}$, (F) resting CD4 memory T and (G) monocyte infiltration in the IMVigor 210 cohort (n=348). SYNPO2, Synaptopodin-2; TPM, Transcript per million; PDL1, Programmed cell death 1 ligand 1; TIDE, Tumor Immune Dysfunction and Exclusion; ns, no significance. *, *** and **** indicate $P<0.05$, $P<0.001$, $P<0.0001$, respectively.
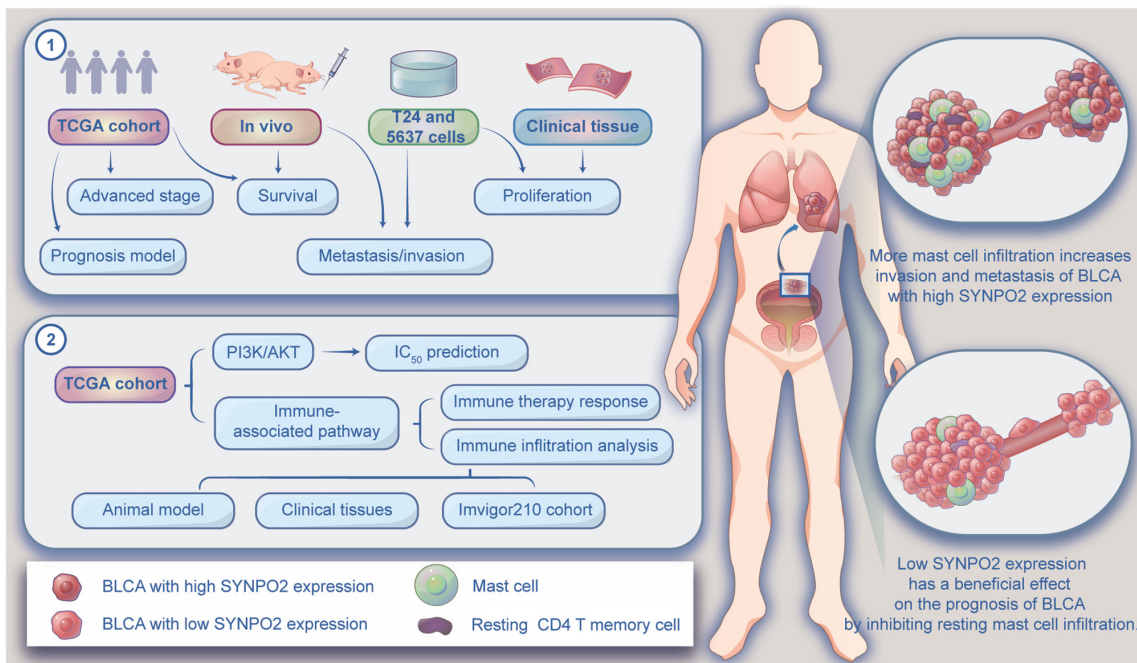

Figure 7. Role of SYNPO2 expression in biological functions and mast cell infiltration. TCGA and clinical tissue analysis and *in vivo* and *in vitro* experiments demonstrated SYNPO2 expression plays a key role in regulating the biological functions of BLCA. Gene enrichment, TIDE and immune infiltration analysis and IC_{50} prediction using TCGA and Imvigor210 cohorts, animal experiments and clinical tissue analysis demonstrated an association between SYNPO2 expression and mast cell infiltration, as well as its implications for BLCA therapy. SYNPO2 expression promoted infiltration of resting mast cells, ultimately leading to the metastasis of BLCA from bladder tissue to the lungs. TCGA, The Cancer Genome Atlas; SYNPO2, synaptopodin-2; IC_{50}, half maximal inhibitory concentration; TIDE, Tumor Immune Dysfunction and Exclusion; BLCA, Bladder Urothelial Carcinoma.

and the gastrointestinal tract. Their degranulation is a fundamental biological process involved in immune responses (47). This process also involves the release of various inflammatory mediators, including TNF-α and β, IL-10, chemokines such as CXCL10 and CXCL8, as well as other factors such as histamine. It serves a pivotal role in recruiting and regulating immune cells

within the tumor microenvironment (48). Certain studies suggest that mast cells exert anti-tumor effects by secreting inflammatory factors that recruit CD4/CD8^{+} T and NK cells (49,50). However, other evidence indicates that higher mast cell density in bladder cancer is associated with high-grade transitional cell carcinoma (TCC) and serves as a poor prognostic factor for TCC (51). The gradual release of granules from mast cells is associated with immunosuppression and tumor angiogenesis. For example, Visciano *et al* (52) reported that mast cells promote epithelial-mesenchymal transition in cancer tissue by releasing IL-6, VEGF-A and CXCL8. The present study revealed a significant association between SYNPO2 expression and mast cell infiltration, with increased mast cell infiltration being negatively correlated with BLCA survival. Additionally, following PD1/PDL1 immune therapy, SYNPO2 expression is associated with elevated levels of resting and decreased abundance of activated mast cells. In the BLCA mouse model, the high SYNPO2 expression group exhibited significantly increased serum levels of TGF-β1 and IL-6 originating from mast cells. Hence, it was hypothesized that SYNPO2-mediated mast cell infiltration served a crucial role in immunosuppression in BLCA.

Activation of immune checkpoints plays a critical role in immunosuppression within BLCA. Tumor cells often exhibit heightened levels of PD-L1 and B7 ligands that bind to inhibitory receptors such as PD-1 or CTLA-4 on the surface of T cells, thus impairing antigen presentation (53). Jiang *et al* (54) reported that increased PD-1 expression in bladder cancer is linked to reduced 5-year overall and disease-free survival due to disruptions in immune-associated signaling pathways. In a humanized mouse melanoma model, it was observed that the interaction between FOXP3^{+} Treg and mast cells confers resistance to anti-PD-1 treatment (55). In the present study, SYNPO2 exhibited co-expression with immune checkpoint genes such as CTLA-4, PD1 and PDL2 in BLCA and higher SYNPO2 expression was correlated with increased resistance to immune checkpoint inhibitors, indicating the potential role of SYNPO2 in hindering the efficacy of immune therapy by upregulating expression of immune checkpoint genes. These data support SYNPO2 as a promising candidate target for immune therapy in BLCA.

Acknowledgements

Funding

Availability of data and materials

The datasets used and/or analyzed during the current study are available from the corresponding author on reasonable request.

Authors' contributions

YS and XZ designed the study. GY and LT confirmed the authenticity of all the raw data. ZL and XL were involved in data collection, interpretation and analysis. YS and GY performed the literature review and wrote the manuscript. All authors have read and approved the final manuscript.

Ethics approval and consent to participate

The present study was approved by the Institutional Research Ethics Committee of NingBo Medical Center Lihuili Hospital, Ningbo, CHINA (approval no. KY2022PJ024). The animal experiments were approved by Institutional Animal Care and Use Committee, Hangzhou, China; approval no. ZJCLCA-IACUC-20040088).

Patient consent for publication

Not applicable.

Competing interests

The authors declare that they have no competing interests.

References

1. Siegel RL, Miller KD, Wagle NS and Jemal A: Cancer statistics, 2023. CA Cancer J Clin 73: 17-48, 2023.
2. Tran L, Xiao JF, Agarwal N, Duex JE and Theodorescu D: Advances in bladder cancer biology and therapy. Nat Rev Cancer 21: 104-121, 2021.
3. Lenis AT, Lec PM and Chamie K: Bladder cancer. JAMA 324: 2006, 2020.
4. Larsen ES, Joensen UN, Poulsen AM, Goletti D and Johansen IS: Bacillus Calmette-Guérin immunotherapy for bladder cancer: A review of immunological aspects, clinical effects and BCG infections. APMIS 128: 92-103, 2020.
5. Zhao J, Zhou L, Pan Y and Chen L: A systematic review and meta-analysis of radical cystectomy in the treatment of muscular invasive bladder cancer (MIBC). Transl Androl Urol 10: 3476-3485, 2021.
6. Guo CC and Czerniak B: Molecular taxonomy and immune checkpoint therapy in bladder cancer. Surg Pathol Clin 15: 681-694, 2022.
7. Zheng Z and Song Y: Synaptopodin-2: A potential tumor suppressor. Cancer Cell Int 23: 158, 2023.
8. Leinweber BD, Fredricksen RS, Hoffman DR and Chalovich JM: Fesselin: A novel synaptopodin-like actin binding protein from muscle tissue. J Muscle Res Cell Motil 20: 539-545, 1999.
9. Faul C, Dhume A, Schecter AD and Mundel P: Protein kinase A, Ca2+/calmodulin-dependent kinase II, and calcineurin regulate the intracellular trafficking of myopodin between the Z-disc and the nucleus of cardiac myocytes. Mol Cell Biol 27: 8215-8227, 2007.
10. De Ganck A, De Corte V, Bruyneel E, Bracke M, Vandekerckhove J and Gettemans J: Down-regulation of myopodin expression reduces invasion and motility of PC-3 prostate cancer cells. Int J Oncol 34: 1403-1409, 2009.
11. Linnemann A, Vakeel P, Bezerra E, Orfanos Z, Djinović-Carugo K, van der Ven PF, Kirfel G and Fürst DO: Myopodin is an F-actin bundling protein with multiple independent actin-binding regions. J Muscle Res Cell Motil 34: 61-69, 2013.
12. Kai F, Fawcett JP and Duncan R: Synaptopodin-2 induces assembly of peripheral actin bundles and immature focal adhesions to promote lamellipodia formation and prostate cancer cell migration. Oncotarget 6: 11162-11174, 2015.
13. Liu J, Ye L, Li Q, Wu X, Wang B, Ouyang Y, Yuan Z, Li J and Lin C: Synaptopodin-2 suppresses metastasis of triple-negative breast cancer via inhibition of YAP/TAZ activity. J Pathol 244: 71-83, 2018.

14. Roperto S: Role of BAG3 in bovine Deltapapillomavirus-mediated autophagy. J Cell Biochem 123: 59-64, 2022.
15. Faul C, Hüttelmaier S, Oh J, Hachet V, Singer RH and Mundel P: Promotion of importin alpha-mediated nuclear import by the phosphorylation-dependent binding of cargo protein to 14-3-3. J Cell Biol 169: 415-424, 2005.
16. Livak KJ and Schmittgen TD: Analysis of relative gene expression data using real-time quantitative PCR and the 2(-Delta Delta C(T)) method. Methods 25: 402-408, 2001.
17. Love MI, Huber W and Anders S: Moderated estimation of fold change and dispersion for RNA-seq data with DESeq2. Genome Biol 15: 550, 2014.
18. Wu T, Hu E, Xu S, Chen M, Guo P, Dai Z, Feng T, Zhou L, Tang W, Zhan L, et al: clusterProfiler 4.0: A universal enrichment tool for interpreting omics data. Innovation (Camb) 2: 100141, 2021.
19. Geeleher P, Cox N and Huang RS: pRRophetic: An R package for prediction of clinical chemotherapeutic response from tumor gene expression levels. PLoS One 9: e107468, 2014.
20. Aran D, Hu Z and Butte AJ: xCell: Digitally portraying the tissue cellular heterogeneity landscape. Genome Biol 18: 220, 2017.
21. Jiang P, Gu S, Pan D, Fu J, Sahu A, Hu X, Li Z, Traugh N, Bu X, Li B, et al: Signatures of T cell dysfunction and exclusion predict cancer immunotherapy response. Nat Med 24: 1550-1558, 2018.
22. Mariathasan S, Turley SJ, Nickles D, Castiglioni A, Yuen K, Wang Y, Kadel EI III, Koeppen H, Astarita JL, Cubas R, et al: TGFβ attenuates tumour response to PD-L1 blockade by contributing to exclusion of T cells. Nature 554: 544-548, 2018.
23. Wang Y, Ju L, Wang G, Qian K, Jin W, Li M, Yu J, Shi Y, Wang Y, Zhang Y, et al: DNA polymerase POLD1 promotes proliferation and metastasis of bladder cancer by stabilizing MYC. Nat Commun 14: 2421, 2023.
24. Tan TZ, Rouanne M, Tan KT, Huang RY and Thiery JP: Molecular subtypes of urothelial bladder cancer: Results from a meta-cohort analysis of 2411 tumors. Eur Urol 75: 423-432, 2019.
25. Wu X, Lv D, Cai C, Zhao Z, Wang M, Chen W and Liu Y: A TP53-associated immune prognostic signature for the prediction of overall survival and therapeutic responses in muscle-invasive bladder cancer. Front Immunol 11: 590618, 2020.
26. Huang S, Hua X, Kuang M, Zhu J, Mu H, Tian Z, Zheng X and Xie Q: miR-190 promotes malignant transformation and progression of human urothelial cells through CDKN1B/p27 inhibition. Cancer Cell Int 21: 241, 2021.
27. Koch J, Schober SJ, Hindupur SV, Schöning C, Klein FG, Mantwill K, Ehrenfeld M, Schillinger U, Hohnecker T, Qi P, et al: Targeting the Retinoblastoma/E2F repressive complex by CDK4/6 inhibitors amplifies oncolytic potency of an oncolytic adenovirus. Nat Commun 13: 4689, 2022.
28. Chen Z, Chen X, Xie R, Huang M, Dong W, Han J, Zhang J, Zhou Q, Li H, Huang J and Lin T: DANCR promotes metastasis and proliferation in bladder cancer cells by enhancing IL-11-STAT3 signaling and CCND1 expression. Mol Ther 27: 326-341, 2019.
29. Pastushenko I and Blanpain C: EMT transition states during tumor progression and metastasis. Trends Cell Biol 29: 212-226, 2019.
30. Zhang Z, Yu Y, Li P, Wang M, Jiao W, Liang Y and Niu H: Identification and validation of an immune signature associated with EMT and metabolic reprograming for predicting prognosis and drug response in bladder cancer. Front Immunol 13: 954616, 2022.
31. Alzahrani AS: PI3K/Akt/mTOR inhibitors in cancer: At the bench and bedside. Semin Cancer Biol 59: 125-132, 2019.
32. Xing Y, Lin NU, Maurer MA, Chen H, Mahvash A, Sahin A, Akcakanat A, Li Y, Abramson V, Litton J, et al: Phase II trial of AKT inhibitor MK-2206 in patients with advanced breast cancer who have tumors with PIK3CA or AKT mutations, and/or PTEN loss/PTEN mutation. Breast Cancer Res 21: 78, 2019.
33. Hu W, Zhang Y, Ning J, Li M, Tang Y, Li L, Cheng F and Yu W: Anti-tumor effect of AZD8055 against bladder cancer and bladder cancer-associated macrophages. Heliyon 9: e14272, 2023.
34. Camidge DR, Otterson GA, Clark JW, Ignatius Ou SH, Weiss J, Ades S, Shapiro GI, Socinski MA, Murphy DA, Conte U, et al: Crizotinib in patients with MET-amplified NSCLC. J Thorac Oncol 16: 1017-1029, 2021.
35. Zou Z, Chen J, Yang J and Bai X: Targeted inhibition of Rictor/mTORC2 in cancer treatment: A new era after rapamycin. Curr Cancer Drug Targets 16: 288-304, 2016.
36. Chen J, Wu S, Peng Y, Zhao Y, Dong Y, Ran F, Geng H, Zhang K, Li J, Huang S and Wang Z: Constructing a cancer stem cell related prognostic model for predicting immune landscape and drug sensitivity in colorectal cancer. Front Pharmacol 14: 1200017, 2023.
37. Sun Y, Chen Y, Zhuang W, Fang S, Chen Q, Lian M, Lv C, Weng J, Wei R, Lin Y, et al: Gastric cancer peritoneal metastasis related signature predicts prognosis and sensitivity to immunotherapy in gastric cancer. J Cell Mol Med: Aug 21, 2023 (Epub ahead of print).
38. Topalian SL, Taube JM, Anders RA and Pardoll DM: Mechanism-driven biomarkers to guide immune checkpoint blockade in cancer therapy. Nat Rev Cancer 16: 275-287, 2016.
39. Bagchi S, Yuan R and Engleman EG: Immune checkpoint inhibitors for the treatment of cancer: Clinical impact and mechanisms of response and resistance. Annu Rev Pathol 16: 223-249, 2021.
40. Gan L, Camarena V, Mustafi S and Wang G: Vitamin C inhibits triple-negative breast cancer metastasis by affecting the expression of YAP1 and synaptopodin 2. Nutrients 11: 2997, 2019.
41. OuYang C, Xie Y, Fu Q and Xu G: SYNPO2 suppresses hypoxia-induced proliferation and migration of colorectal cancer cells by regulating YAP-KLF5 axis. Tissue Cell 73: 101598, 2021.
42. Chang SL, Yang CC, Lai HY, Tsai HH, Yeh CF, Lee SW, Kuo YH, Kang NW, Wu WB and Chen TJ: SYNPO2 upregulation is an unfavorable prognostic factor for nasopharyngeal carcinoma patients. Medicine (Baltimore) 102: e34426, 2023.
43. Chi M, Liu J, Mei C, Shi Y, Liu N, Jiang X, Liu C, Xue N, Hong H, Xie J, et al: TEAD4 functions as a prognostic biomarker and triggers EMT via PI3K/AKT pathway in bladder cancer. J Exp Clin Canc Res 41: 175, 2022.
44. Wang J, Shen C, Zhang J, Zhang Y, Liang Z, Niu H, Wang Y and Yang X: TEAD4 is an immune regulating-related prognostic biomarker for bladder cancer and possesses generalization value in pan-cancer. DNA Cell Biol 40: 798-810, 2021.
45. Li MO, Wolf N, Raulet DH, Akkari L, Pittet MJ, Rodriguez PC, Kaplan RN, Munitz A, Zhang Z, Cheng S and Bhardwaj N: Innate immune cells in the tumor microenvironment. Cancer Cell 39: 725-729, 2021.
46. Yang Z, Zhang B, Li D, Lv M, Huang C, Shen GX and Huang B: Mast cells mobilize myeloid-derived suppressor cells and Treg cells in tumor microenvironment via IL-17 pathway in murine hepatocarcinoma model. PLoS One 5: e8922, 2010.
47. Aponte-López A and Muñoz-Cruz S: Mast cells in the tumor microenvironment. Adv Exp Med Biol 1273: 159-173, 2020.
48. Komi DEA and Redegeld FA: Role of mast cells in shaping the tumor microenvironment. Clin Rev Allerg Immu 58: 313-325, 2020.
49. Dalton DK and Noelle RJ: The roles of mast cells in anticancer immunity. Cancer Immunol Immunother 61: 1511-1520, 2012.
50. Elieh Ali Komi D and Grauwet K: Role of mast cells in regulation of T cell responses in experimental and clinical settings. Clin Rev Allergy Immunol 54: 432-445, 2018.
51. Kim JH, Kang YJ, Kim DS, Lee CH, Jeon YS, Lee NK and Oh MH: The relationship between mast cell density and tumour grade in transitional cell carcinoma of the bladder. J Int Med Res 39: 1675-1681, 2011.
52. Visciano C, Liotti F, Prevete N, Cali' G, Franco R, Collina F, de Paulis A, Marone G, Santoro M and Melillo RM: Mast cells induce epithelial-to-mesenchymal transition and stem cell features in human thyroid cancer cells through an IL-8-Akt-Slug pathway. Oncogene 34: 5175-5186, 2015.
53. Morad G, Helmink BA, Sharma P and Wargo JA: Hallmarks of response, resistance, and toxicity to immune checkpoint blockade. Cell 185: 576, 2022.
54. Jiang LR, Zhang N, Chen ST, He J, Liu YH, Han YQ, Shi XQ, Yang JJ, Mu DY, Fu GH and Gao F: PD-1-positive tumor-associated macrophages define poor clinical outcomes in patients with muscle invasive bladder cancer through potential CD68/PD-1 complex interactions. Front Oncol 11: 679928, 2021.
55. Somasundaram R, Connelly T, Choi R, Choi H, Samarkina A, Li L, Gregorio E, Chen Y, Thakur R, Abdel-Mohsen M, et al: Tumor-infiltrating mast cells are associated with resistance to anti-PD-1 therapy. Nat Commun 12: 346, 2021.